GelSlim 3.0: High-Resolution Measurement of Shape, Force and Slip in a Compact Tactile-Sensing Finger

Ian H. Taylor Siyuan Dong Alberto Rodriguez
Massachusetts Institute of Technology

***Abstract*— This work presents a new version of tactile-sensing finger, GelSlim 3.0, which integrates the ability to sense high-resolution shape, force, and slip in a more compact form factor than previous implementations, designed for cluttered bin-picking scenarios. The novel design integrates real-time model-based algorithms to measure shape, estimate the 3-D contact force distribution, and detect incipient slip. The constraints imposed by the photometric stereo algorithm used for depth reconstruction and the implementation of a planar sensing surface make the miniaturization of previous designs nontrivial. To achieve a compact integration, we optimize the optical path from illumination source to camera. Using an optical simulation environment, we develop an illumination shaping lens and position the source LEDs and camera. The optimized optical configuration is integrated into a finger design composed of a robust and easily replaceable snap-to-fit fingertip module that facilitates manufacture, assembly, use, and repair. To stimulate future research in tactile-sensing and provide the robotics community access to a reliable and easily reproducible tactile finger with a diversity of sensing modalities, we open-source the design, fabrication methods, and software at https://github.com/mcubelab/gelslim.**

I. Introduction

Touch is an essential sensing modality for interfacing with the world. It provides a direct and powerful mechanism for reacting to the environment and is present in almost all biological systems but missing from most robotic ones. We are particularly motivated by the potential of tactile feedback to sense and control the complex contact interactions that occur while manipulating objects within an environment.

This paper presents GelSlim 3.0, a new version of the tactile-sensing finger GelSlim [1], which has been designed for grasping in cluttered environments, and integrates real-time high spatial resolution measurement of shape, force, and slip, in a more compact form factor that is easier to fabricate, utilize and maintain. We present four main contributions.

- **Design:** GelSlim 3.0 is the product of an optimization of the optical path, from illumination source to camera, around the constraints imposed by the photometric stereo algorithm used for depth reconstruction in vision-based tactile sensors [2]. In particular, we optimize the placement of the illumination sources and the geometry of a light shaping lens to enable a compact form factor integration while retaining the ability to reconstruct depth. We evaluate the novel tactile-sensing finger compared to current tactile sensor designs and discuss our implementation's trade-offs and limitations.
- **Manufacturing:** We utilize accessible manufacturing methods to fabricate a new tactile-sensing finger, which is assembled out of a small number of components with a simple and modular snap-to-fit design.
- **Functionality:** The tactile sensor integrates the capability to use real-time model-based algorithms to measure and reconstruct 3D geometry, detect incipient slip, and estimate the spatial distribution of 3D contact forces.
- **Open-Source:** We open-source the design to encourage the proliferation of tactile-sensing technology within the robotics community and to help address some of the many bottlenecks of tactile-sensing in robotics, including manufacture, distribution, and use [3].

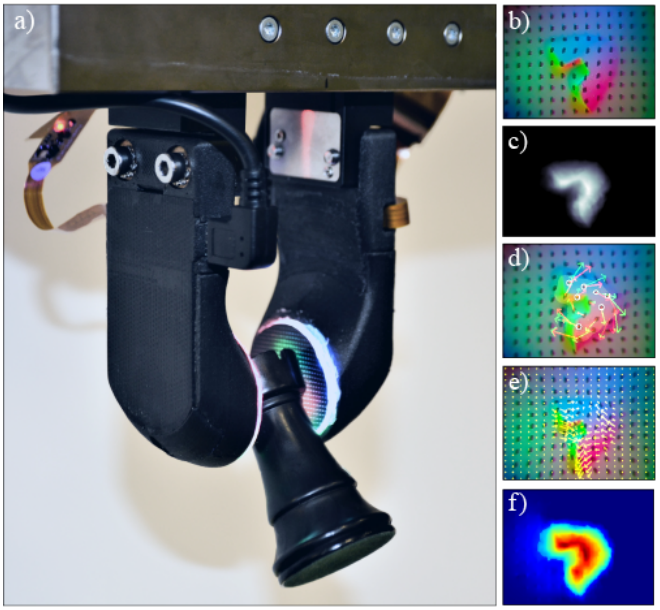

Fig. 1. (a) GelSlim 3.0 sensors grasping a chess rook and the respective tactile imprint and measurement results. (b) High-Resolution Tactile Image (c) Depth Reconstruction (d) Incipient Slip (e) Tangential Force Field (f) Normal Force Field.

This paper is structured as follows: We review related works in tactile-sensing in Section II and discuss the design goals in Section III. We describe the optimization and integration of the optomechanical design components in Section IV and demonstrate the sensing capabilities of resultant tactile-sensing finger in Section V. We compare the novel design to other current tactile-sensing designs and discuss its limitations in Section VI. Finally, we briefly summarize the contributions of the paper in Section VIII.

This work was supported by the NEC Corporation Fund for Research in Computers and Communications, and by the HKSAR Innovation and Technology Fund (ITF) ITS-104-19F. We thank Synopsys, Inc. for providing an educational license for the LightTools Illumination Design Software.

Project repository with details and tutorials on simulation, design, fabrication, and assembly of the sensor: https://github.com/mcubelab/gelslim
Project video: https://www.youtube.com/watch?v=Y10XN9byO0g

II. Related work

Different Versions of Tactile Sensor Figure

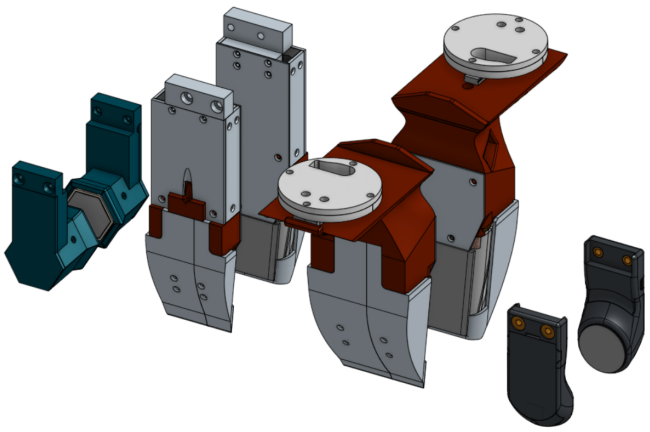

Fig. 2. Models of previous and current integrated tactile sensors (*from left to right*): GelSight [2], GelSlim 2.0 [4], GelSlim MPalm [5], and GelSlim 3.0.

A. GelSight Sensors

GelSight is a vision-based retrographic tactile sensor that makes measurements by using a camera to capture high-resolution images of the surface deformation of an elastomer with opaque skin. The elastomer is illuminated from different directions by color LEDs; the resultant colored shading is used to make direct measurements of the position, shape, and 3D geometry of objects contacting the surface. These types of sensors have become popular within the robotics literature due to their ability to capture contact state feedback with high spatial resolution while maintaining a compact instrumentation [1]. The continued development and improvement of these sensors have yielded several designs that offer compactly integrated and rugged form factors [1], [3], where previously they had been more bulky and/or fragile [6], [7], [2].

Donlon et al. [1], [4] improved upon Dong et al.'s [2] fingertip version of GelSight by altering the optical path to use a waveguide to route light through the fingertip and a mirror to view the sensor surface from a distance, allowing for a more compact wedge-shaped fingertip design, suitable for cluttered picking scenarios. Wilson et al. [8] demonstrated a fully actuated two-finger gripper with multiple GelSight tactile sensors, which were used to measure the surface topology of an object across multiple views simultaneously and track the shear and and tensile stresses. Sensors similar to GelSight and GelSlim that utilize rich 2D and 3D data have been successfully applied in robotic manipulation. Li et al. [9] utilized GelSight fingertip in tandem with a feature-based matching technique to localize and perform an insertion task with small parts held in a robot hand. Tian et al. [10] Proposed and demonstrated an unsupervised learning framework, deep tactile MPC, to learn a predictive model from raw tactile sensor inputs for performing servoing tasks with a GelSight-style tactile sensor. Hogan et al. [5] explored the use of tactile feedback measured by a palm-shaped GelSlim sensor to develop robust primitives with the ability to handle external perturbations and account for object pose uncertainty. Bauza et al. [11] utilized GelSlim sensors to reconstruct the shape of objects from tactile imprints and accurately localize previously reconstructed objects. She et al. [12] demonstrated the ability to manipulate flexible cables by pairing grip and pose controllers that utilized depth and shape feedback from a GelSight sensor to regulate cable sliding dynamics.

B. Other Vision-Based Tactile Sensors

Vision-based tactile sensing approaches are synergistic with deep learning techniques, which have been demonstrated to provide robust and descriptive interpretations of high-dimensional data. There is a diversity of sensor designs that rely more heavily on these methods. For example, She et al. [13] demonstrated an exoskeleton covered soft continuum finger that utilized a convolutional neural network to predict the finger's position. Padmanabha et al. [14] used a thumb-shaped tactile sensor, OmniTact, paired with a ResNet-based neural network to perform tactile state estimation for a representative insertion task. While the number of vision-based tactile-sensing designs continues to increase, Lambeta et al. [3] notes the dearth of sensors that simultaneously fulfill the requirements of being 1) high resolution, 2) highly sensitive, 3) reliable, 4) easy to use, 5) compact and 6) inexpensive. To resolve this bottleneck impeding the widespread adoption of touch sensing in robotic manipulation, they released an open-source tactile sensor Digit that fulfills these criteria.

III. Design Goals

The use of model-based photometric stereo techniques to measure 3D geometry is a primary influence on the configuration and position of the optical elements within a tactile sensor [1]. The decision to incorporate these techniques constrains the design space as it requires that at least three colors of light be directed across the gel from different directions [15]. These requirements also enforce geometric constraints that affect feasible camera placement and illumination paths. For example, the need for multiple evenly distributed illumination channels encourages designs that position luminaries in a radially symmetric configuration. Limitations of the focal length of the available cameras constrain the maximum field of view possible, and thus, the sensing area for a given sensor thickness. A comprehensive review of the tactile design space constraints can be found in [1]. These constraints often prove challenging and counterproductive to slim robotic finger integrations [1]. While previous implementations of GelSlim have eschewed model-based reconstruction techniques in favor of relaxing the design space constraints [1], [4], these techniques continue to prove useful for complex manipulation scenarios [12].

Previous designs of GelSight and GelSlim, while cost-effective, have been difficult to manufacture and assemble en-masse or by inexperienced users due to their reliance on complex by-hand fabrication techniques that are incompatible with retail fabrication services (e.g., acrylic waveguide bending, custom hand-soldered luminaries)[3], [1], [16], [2].

To address these issues while maintaining the strengths of previous GelSight and GelSlim designs, we present the following design goals for the proposed tactile finger:

- **Compactness** of the finger allows access to and precise placement of objects in clutter by squeezing between objects or separating them from the environment.
- **model-based Measurement Methods** utilized in previous high-resolution camera-based tactile sensors provide multiple types of rich contact state feedback (raw high-resolution images, shape, force, and slip) at real-time speeds without requiring data-expensive calibration or learning procedures. These provide a strong basis for novel methods of dexterous manipulation and control.
- **Design for Assembly (DFA)** enforces robust and modular design practices that make the fabrication and utilization of the proposed tactile finger accessible to a broader range of the robotics research community.

The following sections give a detailed description of the process to use these design goals to select and optimize the optical (Section IV-A), electrical (Section IV-B), and mechanical (Section IV-C) design parameters. Finally, we describe the fabrication and assembly of the tactile finger (Section IV-D).

IV. Design of GelSlim 3.0

A. Optical Design

The use of photometric stereo techniques is a primary influence on the constraints of a tactile sensor's optical design space. Therefore, we briefly review the photometric stereo algorithm and its assumptions (IV-A.1). We evaluate these restrictions paired with the proposed design goals to set the initial conditions for the design space (IV-A.2). We then generate a raytracing simulation of an initial optical path using illumination design software, identify design optimization parameters (IV-A.3) and generate an optimized optical configuration using the software's built-in optimizer (IV-A.4).

1) Photometric Stereo: Our implementation of photometric stereo relies on the same techniques first described by Johnson et al. [15] and used in the original GelSight sensor design as a way to perform model-based reconstruction of the deformation of an elastomer in 3D. The technique assumes the following three conditions:

1) The image seen by the vision system is an orthographic projection of the sensor surface, i.e. every point in the image corresponds to a point on the sensor surface. Thus, the gradients of the surface deformation can be defined as the partial derivatives at those points.
2) The shading at any point in the image is a function of the surface normal of the sensing surface; this effectively assumes no cast shadows or interreflections.
3) The proportion of incident light reflected (albedo) is constant across the sensor's surface.

To reconstruct the surface normals, we determine the mapping between the intensity at each pixel and the reflectance function. Theoretically, many sets of gradients will correspond to a set of intensity values; therefore, the reflectance function is not trivially invertible. For this reason, the photometric stereo technique uses images captured under different illumination conditions (from three differently colored channels). The three measurements per pixel over-constrain the problem and allow us to estimate the two gradient values. We measure the intensity using an object of a known shape, e.g., a sphere with a known radius. From the data, we generate a lookup table; which serves as the method of inversion. Finally, we use a fast Poisson solver to integrate the surface gradient and reconstruct the depth.

While this method does not assume point light sources [15], we incorporate illumination homogeneity as a second-order assumption. Inhomogeneous behavior, e.g., areas with intensity variance and missing illumination, will reduce the depth reconstruction accuracy. The former will disproportionately skew the gradient function, and the latter will reduce the number of measurements per pixel, making the reflectance-intensity mapping not trivially invertible and will generate incorrect depth values.

2) Initial Conditions: To satisfy the photometric stereo assumptions, we select the initial design parameters based on previous designs of GelSight and GelSlim as well as our design goals. We discuss the effects our selections have on the design space.

- **Camera:** We choose a Raspberry Pi 160° variable focus wide-angle camera module (ODSEVEN) as it is an inexpensive and compact camera that provides a large field of view and a close minimum focus distance. We cannot completely satisfy the orthographic assumption as the camera's output is warped due to the spherical distortion induced by the wide-angle lens; thus, while all points in the image correspond to a point on the sensing surface, they are not orthographic projections of one another. We address this discrepancy in Section V-A by performing a pre-processing step that removes the wide-angle distortion.
- **Shaping Lens:** We select a hexagonal prism with an angled loft as the basis for the initial lens geometry. The hexagonal shape naturally satisfies the needs of the photometric stereo algorithm used with three illumination channels by providing radially symmetric illumination, which induces the required constraints on the reflectance function [15]. We scale the initial lens geometry to maximize the camera modules' field of view and, thereby, the total sensing area while constraining the maximum finger thickness to be 20 mm. We choose this constraint based on our observations of compact grippers commonly used in industrial pick-and-place applications. Because this assumption is mainly affected by the lens geometry we address our approach to fulfilling its requirements in the subsequent section when selecting the illumination shaping feature's optimization parameters.
- **Gel Shape:** The light distribution is affected by the curvature of the sensing surface. Previous tactile sensors capable of model-based depth reconstruction using photometric stereo have had to use parabolic and spherically curved surfaces to properly fulfill the technique's assumptions at the cost of increased grasp complexity [2]. We select a planar surface paired with a shaping lens to simplify grasping and allow the fingers to more readily grasp objects lying flush on flat surfaces [17].

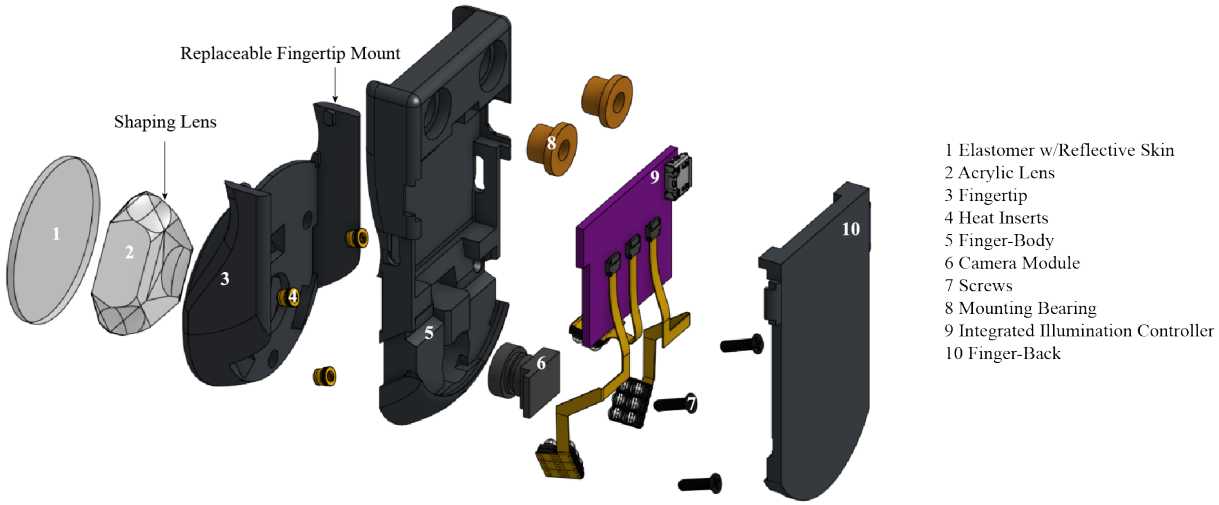

Fig. 3. Exploded diagram of the GelSlim 3.0 tactile finger and its 10 components

- **Gel Material:** We select an elastomer skin with Lambertian reflectance that provides a uniform and diffuse albedo. This enables measurements of the surface normal which are more precise than measurements with a semi-specular albedo[2].
- **Illumination** Using a Lambertian reflectance skin limits the design space as the intensity of light reflected by the diffuse albedo is too low to effectively use total internal reflection (TIR) techniques to route and distribute the light across the surface; a technique used in previous versions of GelSlim and GelSight with semi-specular skin [1], [16]. As a result, the luminaries must directly illuminate the elastomer's surface, and the optical design must incorporate alternative methods to illuminate the sensor's surface homogeneously. We aim to accomplish this by optimizing the light distribution with an illumination shaping lens.

3) Simulation and Parameter Selection: We simulate the optical system configured by the initial conditions using Synopsys LightTools Illumination Design Software linked to a Solidworks CAD model of the shaping lens; this allows us to use Solidworks geometric feature parameters directly as optimization variables. To accurately simulate the optical system we consider the following:

- **Material Parameters:** To model the ray interactions between different materials, we set the refractive indices and reflectance of each optical component using built-in material profiles.
- **Data Collection:** We place a forward simulation receiver on the modeled sensing surface to collect intensity and color distribution data.
- **Source Models:** To simulate the selected photodiodes, we use the source models provided by the luminary manufacturer, which contain their package CAD, source distribution, and spectral region data.
- **Emittance:** To model an intensity-matched ideal photometric stereo system, we match radiometric power for all sources.

We performed proof of concept testing to constrain the design space and select the lens shape and LED package type. We find that a hybrid swept spline lens distributes the illumination intensity more homogeneously than a lens with flat sides 5 while inducing fewer interreflective visual artifacts than planar or spherical convex and concave lenses. Additionally, we find that a 60° viewing angle PLCC-4 Package OSRAM TOPLED Black T66 series LED provides an illumination profile that is diffuse yet easily shaped. We initialize the optimization in Eq.(1) according to the features of the design space seen in Fig. 4:

$$
\begin{aligned}
&\textit{Given} \quad \overline{\mathbf{A}} = [\mathbf{x}, \mathbf{y}, \mathbf{z}, \alpha], \ \overline{\mathbf{B}} = [\mathbf{L}, \theta, \mathbf{R_1}, \mathbf{R_2}, \mathbf{R_3}] \\
&\textit{minimize} \quad f(\overline{A}, \overline{B}) \\
&\textit{subject to}: \ \mathbf{0} \le \mathbf{z} \le \mathbf{t_1} \quad \textit{and} \quad \sigma(\mathbf{x}, \mathbf{y}) = (\mathbf{0}, \mathbf{0}) \\
&\qquad\qquad\ \ \mathbf{0} \le \mathbf{L} \le \mathbf{t_2} \qquad\qquad \mu_{\mathbf{CIE}}(\mathbf{x}, \mathbf{y}) = (.\overline{\mathbf{33}}, .\overline{\mathbf{33}}) \\
&\qquad\qquad\ \ \mathbf{0} \le \alpha \le \mathbf{90} \qquad\qquad \mathbf{G}(\mathbf{x}, \mathbf{y}) = (\mathbf{0}, \mathbf{0}) \\
&\qquad\qquad\ \ \mathbf{0} \le \theta \le \mathbf{90} \qquad\qquad \mathbf{x} = \mathbf{m_x}, \ \mathbf{y} \ge \mathbf{m_y} \\
&\qquad\qquad\qquad\qquad\qquad\qquad\ \ \mathbf{R_1} \ge \mathbf{0}, \ \mathbf{R_2} \ge \mathbf{0}, \ \mathbf{R_3} \ge \mathbf{0}
\end{aligned}
\tag{1}
$$

Where $\overline{A}$ and $\overline{B}$ represent the LED position and shaping lens parameters, respectively, where x, y, z are the coordinate positions within cartesian space and α is the angle of the LED relative to the top face of the lens. t_1 is the total thickness of the lens, and t_2 is the maximum thickness of the shaping feature. The maximum thickness is constrained to 2 mm to ensure the shaping feature does not extend too far from the sensing surface and increase the finger's total thickness. $m_{x,y}$ is coordinate origin within the shaping feature plane.

In abstract, the cost function $f(\overline{A}, \overline{B})$ represents the design space modeled by the initial optical configurations within the simulator engine. The CIE mean (μ_{CIE}) represents the average chromaticity coordinate value for all bins (i.e., test coordinates) in a receiver mesh, where the X coordinate represents a mix of the three CIE RGB curves and Y represents the luminance value. The goal value designates the chromaticity coordinates of the reference white point (the color coordinates that define the color "white" and thus, the point at which red, green, and blue are mixed homogeneously). Satisfying this goal ensures that the *total* illumination distribution approximates the white point. The

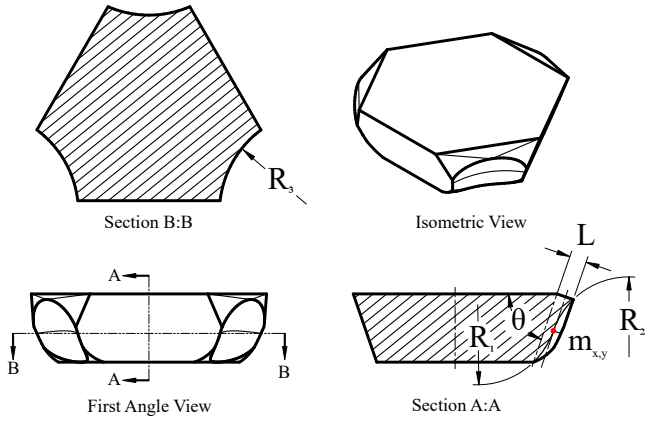

Fig. 4. Diagram of the hybrid swept spline lens with optimization parameters labeled across multiple views. The point $m_{x,y}$ is marked with a red dot.

illuminance mesh standard deviation (σ) goal value incentivizes the intensity to remain constant across the sensing surface. Thus, the optical configuration will maintain a homogeneous and evenly mixed distribution. The illumination centroid ($G(x,y)$) is the position of the arithmetic mean of the intensity distribution across the local receiver bins. The goal value further enforces illumination homogeneity by addressing assumption (2). The goal value incentivizes positioning the centroid at the center of the lens ($G(x,y) = (0,0)$). This directly addresses assumption (2) as it reduces interreflections, which most often occur when high-intensity illumination refracts and reflects while directed at the acute features (ex: sharp corners) often present near the boundary of a lens. Due to the optical configuration's radial symmetry, we can utilize a single parameter set to represent the shaping geometries used for each of the three individual color channels. The full optical configuration is used during the optimization of the proposed minimization problem.

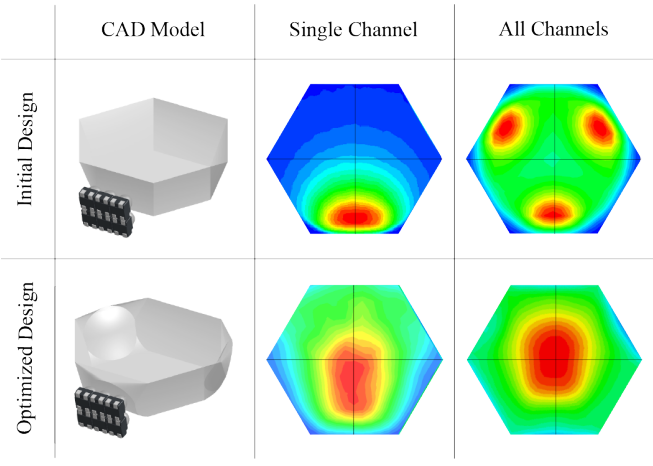

Fig. 5. Heat-maps of the simulated radiant flux across the surface of the sensor before and after optimization plotted using a 25x25 receiver mesh.

4) Optimization Results: The optimizer evaluates as a two-step process where Solidworks configures the lens features based on the optimization variables and initial conditions, and LightTools uses raytracing to simulate the optical system and evaluate the cost function. We plot and display a comparison of the intensity distributions of the initial and final geometries in Fig. 5. The optimized shaping features effectively distribute the illumination across the surface of the sensor. We observe that the full channel distribution of the optimized lens is not entirely radially symmetric; this is likely due to the interreflective artifacts generated within the compact form factor lens. Additionally, while the distribution is improved, it is not ideally homogeneous as there are still portions of the sensing surface near the edges where there are large deviations in the illumination. We find that at the origin coordinate, the optimized design sufficiently satisfies the aforementioned first and second-order assumptions and demonstrates the desired ability to use the photometric stereo algorithm to generate 3D reconstructions with low noise as seen in Fig. 6 and Fig. 9. Reconstructions at the peripheral edges of the sensor are more prone to noisy behavior. This is in comparison with the initial design, which did not produce usable photometric data. We further discuss the finger's resultant capabilities and compare the performance to previous tactile sensor designs in Section VI.

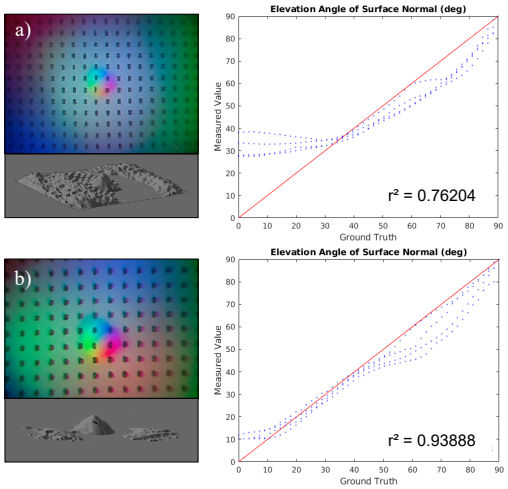

Fig. 6. 3D reconstruction results for the initial (a) and optimized (b) design configurations. Reconstructions were generated after calibrating each sensor configuration with 100 images. The plots compare the measured surface normal angles and ground truth. We find that the optimized sensor measures the surface normal more precisely.

B. Electrical Design

The electrical assembly supplies power to and secures the LED luminaries. The circuit diagram is shown in 7. The resistance values R1, R2, and R3, normalize the three color channel's relative illumination while R0 modulates the total intensity. We use the camera module's spectral transmission profile and manufacturer specifications of the current vs. luminous intensity relationship for each LED to select and tune the channel resistances. The LEDs for each channel are wired as a 3x2 array in parallel to homogenize the illumination and minimize sequential intensity loss across LEDs in a channel.

C. Mechanical Design

The mechanical assembly consists of the fingertip, finger-body, and finger-back. These three components are designed to encapsulate the optical path and provide the most compact

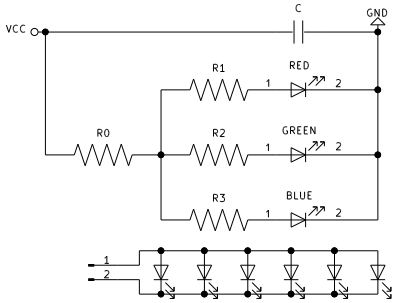

Fig. 7. Circuit diagrams of the Driver PCB (Top) each color channel has its own LED array (Bottom).

form factor possible. The fingertip's distal face is curved, which allows the finger to more readily slip between objects when grasping in clutter. The mounting geometry is designed for use with a Weiss WSG-32 gripper but can be easily adjusted to accommodate various grippers. The fingertip and finger-body are joined with an easily separable sliding rail system in addition to several screws. The respective component cavities of the two bodies maintain press-fit tolerances. In combination, these features allow for easy assembly and maintenance of the sensor, as any component can be accessed and easily removed for replacement if necessary. The modular snap-to-fit mechanical design allows the fingertip to be easily swapped out, if necessary, to switch between task-specific elastomers.

D. Fabrication and Assembly

The finger assembly is composed of ten components as seen in Fig. 3, all of which, except the elastomer, are either 3D printed (Fingertip, finger-body, finger-back), retail made-to-order (Driver PCB, Illumination harness, and acrylic lens) or off the shelf components (camera module, mountain bearings, and M2 Heat Inserts and screws). Once the heat inserts are embedded in the fingertip using a soldering iron, the finger is quickly assembled because of the modular "snap-to-fit" design.

The elastomer is cast using XP565 (Silicones Inc.) platinum-based silicone mixed in a 1:10 ratio of activator to base. After degassing in a vacuum chamber, it is poured into an acrylic mold. Once cured, the reflective layer was painted using a gray silicone ink (Print-On Silicone Ink, Raw Material Suppliers) using a 10:1 ratio of silicone ink to its catalyst. A silicone solvent (NOVOCS Gloss, Reynolds Advanced Materials) is added to dilute the silicone ink in a 1:10:30 ratio of ink catalyst to ink to solvent, and an airbrush is used to spray the material on top of the elastomer. After the reflective layer has cured, tracking markers are added to the elastomer by laser cutting holes in a grid pattern on the elastomer's painted surface and adding black silicone ink. The marker layer is sealed by spraying an additional layer of black silicone ink in a process similar to that of the reflective layer. Finally, the elastomer is cut to shape using a template and then bonded to the acrylic lens and finger-body using silicone sealant (Gorilla Silicone Clear Sealant); the completed sensor is then left to cure for 24 hours.

V. Integrated Algorithms for Tactile-Sensing

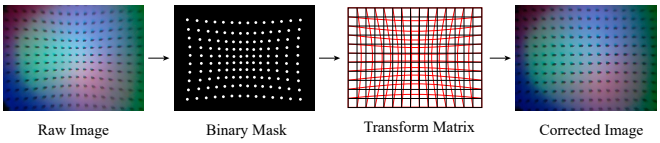

Fig. 8. Diagram of the processing pipeline used to correct spherical lens distortion.

A. Pre-Processing

To sense a physically meaningful contact with the tactile finger, one preprocessing step is needed to correct the optical distortion introduced by the acrylic shaping lens (Part 2 in Fig. 3) and the wide-angle camera module. The distortions in the raw tactile image output can be clearly visualized by the curved marker array in the second image of Fig 8 below. To correct the distortion, we generate a binary mask from the raw tactile image to separate the marker array from the background and detect each marker's position. Using the marker array's known distribution, we calculate the correspondence between each marker in the distorted image and its true position. We interpolate this correspondence across all pixels in the raw image to find the transformation matrix that will reverse the distortion.

B. Shape and Geometry

We described the photometric stereo reconstruction algorithm and its assumptions previously in Section IV-A.1. Fig. 9 demonstrates these capabilities and shows the measured RGB image and the reconstructed depth map of some daily objects touched. The local 3D geometry of the object measured by GelSight/GelSlim sensor has been demonstrated to be useful for object pose estimation [12], [11].

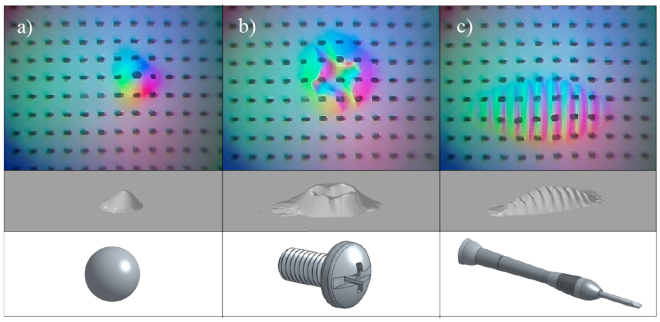

Fig. 9. Raw tactile imprints and their respective 3D reconstructions. Ball Bearing (a) Screw Head (b) Screwdriver Handle (c).

C. Shear and Incipient Slip

Utilizing the method proposed by Dong et al. [18] an approximated shear force [12] can be estimated by tracking the motion of the marker array. By analyzing the coherency of the marker motion field, we can also predict slip.

The core idea is to distinguish whether the sensor surface's motion during contact is consistent with a rigid body motion or not. When the object and sensing surface are in stiction, the surface contact patch and the object move together as a rigid body. When the object is going to slip, some portion of the surface contact patch starts losing stiction with the object, and the motion of the contact surface is no longer a rigid body motion.

We first detect the contact region in the tactile image by selecting the region with a depth that exceeds a preset threshold. We track the markers' motion in the contact region as the "real" motion of the sensor surface in contact. We then calculate the marker motion's rigid body transformation matrix in contact and get the "estimated" motion of the sensor surface under rigid body constraints. A significant deviation between the "real" and "estimate" motion field represents incipient slip. Fig. 10 shows incipient slip detection with the tactile images captured while a chess piece is rotated in the grasp.

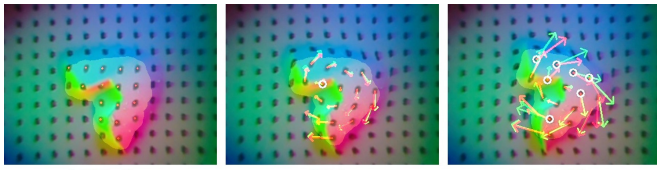

Fig. 10. The evolution from stable contact to incipient slip while the object is being rotated. We label the contact region with yellow, "real" marker tracking with red arrows, "estimate" marker tracking with green arrows, and slipping regions (markers) with a white circle.

D. Dense Force Distribution

To measure an accurate force field, we correspond the gel surface's motion field (measured by tracking the 2D marker motion) and the gel's deformation in the z-axis (depth image) to the force field paired with the FEM model of the gel. The method to do so, proposed by Ma et al. [4] and implemented in GelSlim 2.0, can be augmented using the depth reconstruction offered by the novel GelSlim 3.0 sensor.

We discretize the gel using m 8-node hexahedron elements, where the displacements of the 8 nodes represent the deformation of one FEM element. We calculate the displacement δ_x, δ_y of the 4 nodes on the top by interpolating the marker motion field, the displacement δ_z with the depth map measurement. The δ_x, δ_y need to be adjusted based on the viewing angle between the node-camera frame and δ_z. We use standard FEM theory to calculate the stiffness matrix K with the 8-node hexahedron elements and measured Young's Modulus and Poisson's ratio of the gel. The force field then can be directly calculated with the following equation:

$$F = KU \tag{2}$$

where U is the displacement matrix of all nodes which are directly observable. We show the marker motion field, dense shear force, and the normal force field in Fig. 11 when the sensor is holding a twisted chess piece.

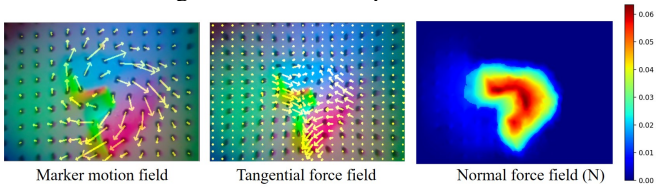

Fig. 11. The marker motion field, tangential force field and normal force field (N)

VI. Discussion

We compare the design components of our sensor with other similar sensors in Table I. We find that our design provides a form factor with comparable thickness and price point to the smallest available sensor Digit while providing a sensing area that is twice as large. This is achieved while incorporating all sensing modalities found in previous versions of GelSight and GelSlim.

A. Design Comparison, Limitations and Trade-offs

TABLE I

Comparison of GelSlim 3.0, GelSlim 2.0, GelSight, Digit and Omnitatct. (*Considering the manufacturing of 1000 pieces)

	GelSlim 3.0	GelSlim 2.0 [4]	GelSight [2]	Digit [3]	Omnitact [14]
Size [mm]	37X80x20	50x172x25	40x80x40	20x27x18	30x30x33
Weight [g]	45	222	NA	20	NA
Sensing Field [mm^2]	675	1200	252	304	3110
Image Resolution	640x480	640x480	640x480	640x480	400x400
Image FPS	90	90	30	60	30
Cost Components [$]	25*	NA	30	15*	600

The trade-offs demonstrated by the optimized sensor are generalizable to tactile sensors' design in other form factors. Thus, they are important lessons to keep in mind for future designs. First and foremost is the use of planar sensing surfaces alongside photometric stereo. In this instance, the sensing surface was not used to shape the illumination to enable grasping from flush surfaces. Although we demonstrated the ability to integrate these two design features using shaping methods, it came at the cost of significantly constraining the design space. We would like to explore alternative methods of fulfilling the photometric stereo assumptions to achieve more compact integration. For example, shaping the illumination directly at the source by using custom-designed microlenses.

Next is the relationship between the camera module's size, the field of view, and the sensor's thickness. To further minimize the form factor, the field of view must be reduced. We used a wide-angle fish-eye lens as a workaround to this trade-off, but this and other methods, for example, utilizing more than one camera, often come at a processing cost. Most image processing software pipelines are sufficiently advanced such that the cost-reward relationship is favorable but this may quickly diminish when using alternative workarounds, for example, utilizing more than one camera to view the sensing surface. In this instance, the cost-reward relationship is less favorable due to the amount of high-dimensional data that needs to be processed.

Finally, is the influence of compactness on the second assumption of the photometric stereo algorithm. It is clear from our results that while interreflections can be minimized through shaping methods and absorptive coatings (in our case marker ink), they cannot be entirely eliminated, and thus they will add some residual noise within the reconstruction. While our design can capture texture information, the features have to be relatively large. This is in comparison with the previous versions of GelSight, which could easily reconstruct micro geometry and surface textures [19], [2], [20], [15]. That being said, left unaccounted for, this interreflective behavior will inhibit the ability to further minimize the sensor thickness in future designs that aim to utilize photometric stereo depth reconstruction.

VII. Open-Source Tactile-Sensing Finger

On the GelSlim Github, we provide documentation, design schematics, and production files (.gbr, .step) for all of the requisite components needed to fabricate a sensor. We also provide a simple software GUI to interface with the sensor and a tutorial describing a data collection system's setup using a Raspberry Pi. The software provides easy access, and use of the three integrated tactile-sensing algorithms described (depth reconstruction, dense force distribution and incipient slip detection) and incorporates the ability to collect, measure and plot tactile imprint data in real-time.

VIII. Conclusions

We present a novel GelSlim tactile finger design and develop the design using illumination design software and design for assembly techniques to analyze, explore, and optimize the finger within its design space. Specifically, we evaluate the effect of incorporating photometric stereo measurement techniques on the design space and demonstrate methods to optimize illumination shaping features to fulfill its assumptions. We develop a compact form factor with replaceable modules suited for grasping in cluttered bin picking scenarios that are easy to manufacture, use, and maintain. We demonstrate that our sensor can utilize all measurement methods used by previous GelSight and GelSlim sensors, specifically 3D depth reconstruction, incipient slip and shear detection, and dense force distribution estimation. We compare our sensor to several other similar tactile-sensing designs and discuss its limitations. We anticipate our future work to continue exploring and developing illumination shaping designs suited explicitly for model-based tactile measurement methods.

References

[1] E. Donlon, S. Dong, M. Liu, J. Li, E. Adelson, and A. Rodriguez, "Gelslim: A high-resolution, compact, robust, and calibrated tactile-sensing finger," in *2018 IEEE/RSJ International Conference on Intelligent Robots and Systems (IROS)*, 2018, pp. 1927–1934.

[2] S. Dong, W. Yuan, and E. H. Adelson, "Improved gelsight tactile sensor for measuring geometry and slip," *2017 IEEE/RSJ International Conference on Intelligent Robots and Systems (IROS)*, Sep 2017. [Online]. Available: http://dx.doi.org/10.1109/IROS.2017.8202149

[3] M. Lambeta, G. Kammerer, D. Jayaraman, R. Calandra, P.-W. Chou, S. Tian, B. Yang, B. Maloon, V. Most, D. Stroud, R. Santos, and A. Byagowi, "Digit: A novel design for a low-cost compact high-resolution tactile sensor with application to in-hand manipulation," *IEEE Robotics and Automation Letters*, vol. PP, pp. 1–1, 02 2020.

[4] D. Ma, E. Donlon, S. Dong, and A. Rodriguez, "Dense tactile force estimation using gelslim and inverse fem," in *2019 International Conference on Robotics and Automation (ICRA)*, 2019, pp. 5418–5424.

[5] F. R. Hogan, J. Ballester, S. Dong, and A. Rodriguez, "Tactile dexterity: Manipulation primitives with tactile feedback," in *2020 IEEE International Conference on Robotics and Automation (ICRA)*, 2020, pp. 8863–8869.

[6] C. Chorley, C. Melhuish, A. Pipe, and J. Rossiter, "Development of a tactile sensor based on biologically inspired edge encoding," *2009 International Conference on Advanced Robotics*, pp. 1–6, 2009.

[7] R. Li, R. Platt, W. Yuan, A. T. Pas, N. Roscup, M. Srinivasan, and E. Adelson, "Localization and manipulation of small parts using gelsight tactile sensing," in *IROS*, 2014.

[8] A. Wilson, S. Wang, B. Romero, and E. Adelson, "Design of a fully actuated robotic hand with multiple gelsight tactile sensors," 2020.

[9] R. Li, R. Platt, W. Yuan, A. ten Pas, N. Roscup, M. A. Srinivasan, and E. Adelson, "Localization and manipulation of small parts using gelsight tactile sensing," in *2014 IEEE/RSJ International Conference on Intelligent Robots and Systems*, 2014, pp. 3988–3993.

[10] S. Tian, F. Ebert, D. Jayaraman, M. Mudigonda, C. Finn, R. Calandra, and S. Levine, "Manipulation by feel: Touch-based control with deep predictive models," in *2019 International Conference on Robotics and Automation (ICRA)*, 2019, pp. 818–824.

[11] M. Bauza, O. Canal, and A. Rodriguez, "Tactile mapping and localization from high-resolution tactile imprints," in *2019 International Conference on Robotics and Automation (ICRA)*, 2019, pp. 3811–3817.

[12] Y. She, S. Wang, S. Dong, N. Sunil, A. Rodriguez, and E. Adelson, "Cable manipulation with a tactile-reactive gripper," 2020.

[13] Y. She, S. Q. Liu, P. Yu, and E. Adelson, "Exoskeleton-covered soft finger with vision-based proprioception and tactile sensing," in *2020 IEEE International Conference on Robotics and Automation (ICRA)*, 2020, pp. 10 075–10 081.

[14] A. Padmanabha, F. Ebert, S. Tian, R. Calandra, C. Finn, and S. Levine, "Omnitact: A multi-directional high-resolution touch sensor," in *2020 IEEE International Conference on Robotics and Automation (ICRA)*, 2020, pp. 618–624.

[15] M. Johnson and E. Adelson, "Retrographic sensing for the measurement of surface texture and shape," in *2009 IEEE Conference on Computer Vision and Pattern Recognition*, 07 2009, pp. 1070 – 1077.

[16] R. Li and E. Adelson, "Sensing and recognizing surface textures using a gelsight sensor," *2013 IEEE Conference on Computer Vision and Pattern Recognition*, pp. 1241–1247, 2013.

[17] A. Zeng, S. Song, K.-T. Yu, E. Donlon, F. R. Hogan, M. Bauza, D. Ma, O. Taylor, M. Liu, E. Romo, N. Fazeli, F. Alet, N. C. Dafle, R. Holladay, I. Morona, P. Q. Nair, D. Green, I. Taylor, W. Liu, T. Funkhouser, and A. Rodriguez, "Robotic pick-and-place of novel objects in clutter with multi-affordance grasping and cross-domain image matching," *The International Journal of Robotics Research*, vol. 0, no. 0, p. 0278364919868017, 0.

[18] S. Dong, D. Ma, E. Donlon, and A. Rodriguez, "Maintaining grasps within slipping bounds by monitoring incipient slip," in *2019 International Conference on Robotics and Automation (ICRA)*, 2019, pp. 3818–3824.

[19] R. Li and E. Adelson, "Sensing and recognizing surface textures using a gelsight sensor," 06 2013, pp. 1241–1247.

[20] M. Johnson, F. Cole, A. Raj, and E. Adelson, "Microgeometry capture using an elastomeric sensor," *ACM Trans. Graph.*, vol. 30, p. 46, 07 2011.